A Combination of Molecular Dynamics and Docking Calculations to Explore the Binding Mode of ADS-J1, a Polyanionic Compound Endowed with Anti-HIV-1 Activity

Fabrizio Manetti,[†] Cristina Tintori,[†] Mercedes Armand-Ugón,[‡] Imma Clotet-Codina,[‡] Silvio Massa,[†] Rino Ragno,[§] José A. Esté,[‡] and Maurizio Botta*[,†]

Dipartimento Farmaco Chimico Tecnologico, Università degli Studi di Siena, I-53100 Siena, Italy, Retrovirology Laboratory irsiCaixa, Hospital Universitari Germans Trias i Pujol, Universitat Autonoma de Barcelona, E-08916 Badalona, Spain, and Dipartimento di Studi di Chimica e Tecnologie delle Sostanze Biologicamente Attive, Università di Roma "La Sapienza", piazzale Aldo Moro 5, I-00185 Roma, Italy

Received September 20, 2005

The HIV-1 entry process is an important target for the design of new pharmaceuticals for the multidrug therapy of AIDS. A lot of polyanionic compounds, such as polysulfonated and polysulfated, are reported in the literature for their ability to block early stages of HIV-1 replication. Several studies have been performed to elucidate the mechanism of the anti-HIV-1 activity of sulfated polysaccharides and polyanions in general, including binding to cell surface CD4 and interfering with the gp120−coreceptor interaction. Here, we show molecular modeling investigations on ADS-J1, a polyanionic compound with anti-HIV activity that is able to interfere with gp120−coreceptor interactions. Agreeing with experimental data, computer simulations suggested that the V3 loop of gp120 was the preferential binding site for ADS-J1 onto HIV-1. Moreover, mutations induced by the inhibitor significantly changed the stereoelectronic properties of the gp120 surface, justifying a marked drop in the affinity of ADS-J1 toward an ADS-J1-resistant HIV-1 strain.

INTRODUCTION

The current agents for the treatment of the human immunodeficiency virus type 1 (HIV-1) infection target three virally encoded proteins and belong to four mechanistic classes, known as entry inhibitors, nucleoside and non-nucleoside reverse transcriptase inhibitors, and protease inhibitors. Mainstay therapy consists of combinations of these agents and is known as highly active antiretroviral therapy (HAART). The impact of HAART has been demonstrated by a significant reduction in AIDS-related mortality. However, the emergence of HIV strains that are resistant to the currently used reverse transcriptase and protease inhibitors has highlighted the need to develop novel antiviral agents with a different mechanism of action. Inhibition of the HIV-1 entry process offers a potentially effective way of meeting this clinical need.[1] The process of HIV-1 entry can be conveniently discussed in the context of three sequentially distinct steps: attachment of the virus to host cells, interaction of the virus with coreceptors, and fusion of the virus with the host cell membranes. In detail, the HIV-1 envelope contains two glycoproteins: gp120, the superficial subunit, and its noncovalently interacting partner, gp41, the transmembrane envelope glycoprotein, which are associated as triple heterodimers.[2,3] The envelope glycoproteins mediate the attachment of HIV-1 to the host cell. The sequential binding of the surface subunit gp120 to the CD4 receptor and a coreceptor, usually CCR5 or CXCR4, induces conformational changes in the envelope glycoproteins. As a consequence of the gp120−coreceptor interaction, the gp41 subunit undergoes a conformational rearrangement, exposing the hydrophobic fusion peptide that inserts into the host cell membrane and initiates the fusion process. The fact that HIV-1 entry is a multistep process allows for the development of anti-HIV-1 drugs that aim at distinct pharmacological targets. A large number of compounds that inhibit the entry stage of virus replication have already been studied,[4] including negatively charged compounds. The heterogeneous nature of polyanionic agents has hindered elucidation of the properties required for their anti-HIV-1 activity. The only common structural denominator appears to be the presence of a sufficient number and adequate density of negative charges. Several different mechanisms have been described to explain the anti-HIV-1 activity of sulfated polysaccharides and polyanions in general, including binding to cell surface CD4[5] and interfering with the gp120−coreceptor interaction.[6−8] Moreover, on the basis of the structure and the positive charge distribution of the V3 loop of gp120 and the development of HIV-1 resistance to several polyanions, it has been predicted that negatively charged compounds will bind to the gp120 and the V3 loop of X4 HIV strains.[4]

ADS-J1 is a polyanionic compound (Figure 1) with potent anti-HIV-1 activity. Previous work had suggested that this compound is able to interact with the hydrophobic cavities on the gp41 central coiled coil and to inhibit complex formation of N/C helices.[9] Moreover, we have recently reported[8] that ADS-J1 was active at blocking HIV-1 replication when tested against viral strains that have been made resistant to the polyanionic entry inhibitor AR177 and cross-resistant to dextran sulfate or the gp41-dependent fusion inhibitor C34. ADS-J1 remained active against HIV strains made resistant to the gp41 fusion inhibitors T20 and C34[10]

* Corresponding author phone: +39 (0)577 234306; fax: +39 (0)577 234333; e-mail: botta@unisi.it.
[†] Università degli Studi di Siena.
[‡] Universitat Autonoma de Barcelona.
[§] Università di Roma "La Sapienza".

10.1021/ci050414h CCC: $33.50
Published on Web 02/03/2006

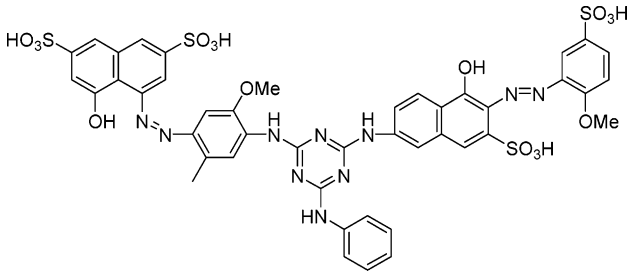

Figure 1. Structure of ADS-J1.

and blocked the binding of the HIV-1 NL4-3 strain (Figure 2) to MT-4 cells but not the binding of HIV-1 NL4-3 that was made resistant to AR177 (thereafter referred to as NL4-3/AR177res), suggesting a distinct mechanism of action of ADS-J1 versus that of other polyanions. In addition, analysis of the molecular target of ADS-J1, by means of the development of drug-resistant variants in a cell culture, demonstrated that resistance to ADS-J1 was not developed through mutations in gp41 but rather in the gp120 coding sequence. Finally, time-of-addition experiments suggested that ADS-J1 interfered with gp120−coreceptor interactions at a time earlier than gp41 inhibitors (T-20 or C34) and later than other polyanions (DS or AR177).[8]

In this context, we have analyzed the molecular target of ADS-J1 by performing both molecular dynamics (MD) and docking simulations. Since the complete three-dimensional structure of gp120 is not available yet, neither from experimental (i.e., X-ray crystallographic or NMR studies) nor theoretical (i.e., computationally generated models) sources, the first goal to be reached by a computational approach was the completion of the gp120 amino acid sequence and its structural optimization. In a first step, the properties of gp120, before and after mutations induced by HIV-1 inhibitors, were studied through the analysis of MD simulations and with calculations of electrostatic potential maps. The last were taken into account on the basis of the fact that variations of the stereoelectronic properties of the gp120 surface were suggested to be a key determinant for the significant loss of affinity of ADS-J1 toward the resistant virus.[8]

In addition, docking studies were next performed to elucidate the binding mode of ADS-J1 and to identify amino acids involved in its mechanism of action. Such calculations were aimed at checking if differences existed in the binding mode of ADS-J1 before and after mutations.

As results of such calculations, V3 and V4 loops were modeled and added to the crystallographic core structure of gp120. Moreover, docking simulations led to the hypothesis that the preferred binding site of ADS-J1 was the V3 loop of gp120, in agreement with experimental data. Finally, variations in the surface charges of the V3 loop seemed to be the major determinant accounting for a different affinity of the ligand toward wild type and mutated enzymes.

COMPUTATIONAL DETAILS

Preparation of the Three-Dimensional Structure of gp120. The X-ray crystallographic structure (2.2 Å resolution, PDB accession code 1g9m)[11] of the monomeric core of gp120 (chain G; residues 83−129, 194−299, 329−397,

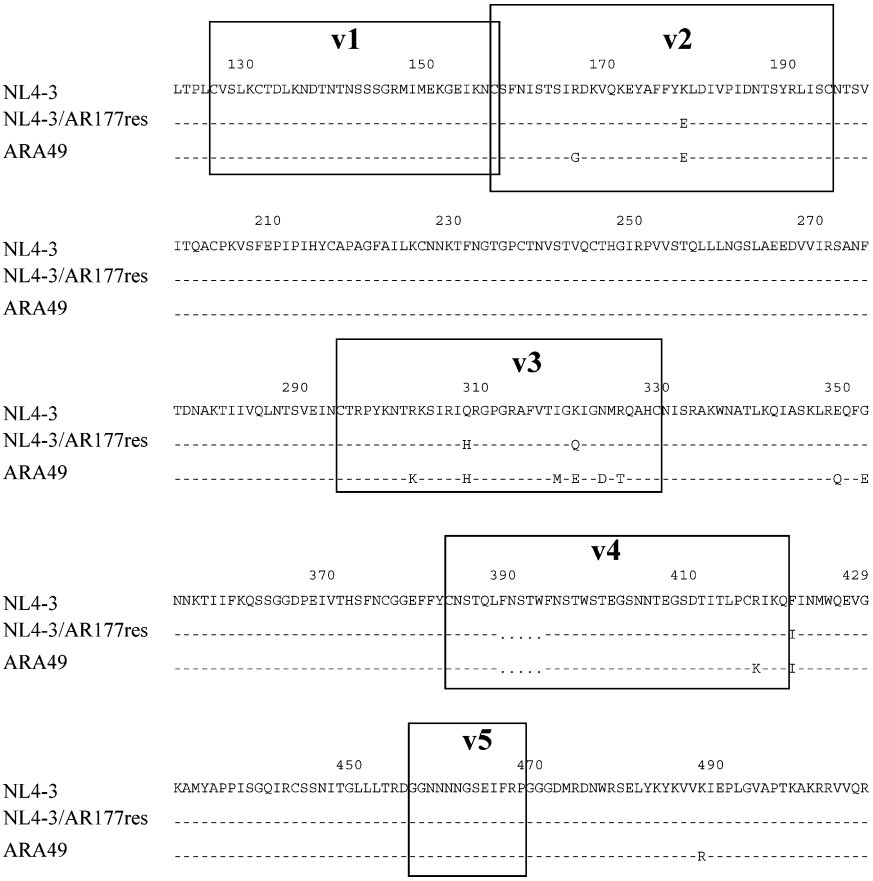

Figure 2. Amino acid sequence of HIV-1 gp120. Numbering in gp120 corresponding to the start coding sequence of the protein in the HXB2 HIV-1 strain. NL4-3/wt is the NL4-3 strain from which AR177 resistance was developed. ARA49 is the NL4-3/AR177-resistant virus passed with ADS-J1. Variable loops of the gp120 are indicated by boxes.

and 410−492), in complex with the two amino-terminal domains of CD4 (D1−D2, chain C, residues 1−181) and the antigen binding fragment (Fab) of the human neutralizing antibody (17b; chains L and H), was chosen as the starting three-dimensional structure for computer simulations. Chains G (gp120) and C (CD4) were included in the calculations, while water molecules; chains L and H; and *N*-acetylglucosamine (NAG), fucose (FUC), and 2-propanol residues were removed. Moreover, the missing V3 and V4 loops were computationally built and added to the core structure of gp120. In detail, V4 was modeled alone by building the corresponding 14-residue peptide (397−410) and submitting it to MD simulations (300 K, water as the solvent), following a computational protocol previously reported to model V4.[12] The distance between Cα atoms of the terminal amino acids 397 and 410, found to be 24.3 Å in the corresponding crystallographic residues, was monitored during the calculations. MD simulations were performed by means of MacroModel (version 8.5)[13] using an AMBER* force field and a distance-dependent electrostatic treatment. Conformations retaining the distance in the range 24.3 ± 0.5 Å were kept for further inspection. Among them, a structure without steric bumps between the V4 loop and the core domain was arbitrarily selected (this choice was based on the fact that the final overall structure of gp120 will be further refined by additional dynamics and minimization calculations. For details, see simulations performed with NAMD software) and integrated into the core domain of gp120 by superposing Cα of the terminal residues of the peptide with the corresponding atoms in the crystallographic structure of gp120.

The V3 loop (298−329 residues) was modeled using the conformations of the 35 amino acid consensus V3 loop (determined by NMR experiments, PDB entry 1ce4)[14] as a template. Such a structure of V3 was aligned to the primary sequence of the V3 loop of NL4-3wt by means of the T-Coffee server.[15] Next, homology modeling calculations were carried out using the SWISS-MODEL, a server for automated comparative modeling of three-dimensional protein structures.[16] Finally, the V3 loop was merged into the assembly constituted by the crystallographic core of gp120 and the modeled V4 loop. Amino acids differing between the gp120 assembly and the NL4-3 wild type (hereafter referred to as NL4-3wt), the HIV-1 strain made resistant to AR177−an HIV entry inhibitor−(NL4-3/AR177res),[17] and the AR177/ADS-J1 double resistant NL4-3 (hereafter referred to as ARA49)[8] sequences were manually changed to obtain three different gp120 structures, in turn optimized through MD simulations to obtain the final sets of atomic coordinates used in all subsequent calculations (see below).

Molecular Dynamics Simulations on Protein Structures. The molecular dynamics package NAMD (version 2.5)[18] and CHARMM22 force field[19] were used for MD simulations of the three computationally built sequences of gp120. Hydrogen atoms were added using the *psfgen* package. Each structure was embedded in a sphere of explicit water molecules with a radius of 71 Å, and the spherical harmonic boundary conditions were applied. The starting structures were relaxed by performing 10 000 steps of conjugate gradient energy minimization to remove unfavorable contacts, followed by 10 000 steps of MD at 310 K (equilibration phase). NAMD was used to perform 720 ps of MD simulations for each system (with complete long-range electrostatic interactions) and with a time step of 2 fs. The temperature was controlled via Langevin dynamics with a dumping factor of 5 ps^{-1}. Snapshot structures were extracted for every 1 ps, resulting in 720 structures from each trajectory. Analyses of the trajectories were performed using the GROMACS software package.[20] Thermodynamic properties, such as temperature and energy, were monitored during MD simulations to check their convergence to stable values. The average structure for each system after equilibration was calculated and submitted to energy minimization by performing 10 000 steps of conjugate gradient.

Generation of the Ligand Structure. The starting structure of ADS-J1 was generated using the program MacroModel. All hydrogens were added to their idealized positions, leaving the sulfonic moieties in the anionic form, thus assigning a total charge of −4 to the ligand. Partial charges were assigned with the MNDO ESP method, and the inhibitor was minimized using an AMBER* force field and the Polak−Ribière conjugate gradient method until the derivative convergence was 0.01 kcal/Å mol.

Molecular Docking of ADS-J1 onto the Protein Structures. To prepare the input structures for docking calculations (Autodock 3.0),[21] complexes between chain C of CD4 and each of the gp120 sequences, as obtained through MD simulations, were further manipulated by removing nonpolar hydrogens, while Kollman united-atom partial charges and solvent parameters were added. Similarly to the protein, the structure of ADS-J1 was also prepared by deleting its nonpolar hydrogen atoms and adding atomic charges obtained with the MNDO ESP method. Finally, the rigid root and rotatable bonds were defined using AutoDockTools.

For blind docking simulations, the structure of gp120 was embedded in a grid box (126 × 94 × 126 Å) centered on the mass center of the protein. The grid spacing (that is, the distance between grid nodes) was set to 0.545 Å. During the next step, several atom probes (characterized by the same stereoelectronic properties as the atoms constituting the inhibitor) were moved on the grid nodes, while the interaction energy between the probe and the inhibitor was calculated at each node. In such a way, grid maps were generated for each atom probe, describing its interactions with the inhibitor. Autogrid 3.0, as implemented in the Autodock software package, was used to generate grid maps.

The Lamarckian genetic algorithm (LGA) was employed to generate orientations or conformations of the ligand within the binding site. The global optimization started with a population of 200 randomly positioned individuals, a maximum of 1.0×10^6 energy evaluations, and a maximum of 27 000 generations. A total of 150 runs were performed, while all the remaining run parameters were maintained at their default settings. A cluster analysis was carried out using 10 Å as the root-mean-square deviation tolerance.

The choice of the best conformation was based on the assumption that, although for high-throughput screening protocols only the first ranked conformation should be considered (that is, the conformation characterized by the lowest estimated free energy of binding),[22] in other cases, the lowest energy conformation of the most populated cluster should also be taken into account.[23]

As a result of blind docking simulations, it was clearly shown that the V3 loop was the preferential binding site of ADS-J1 onto both NL4-3wt and NL4-3/AR177res.

On the basis of these findings and with the aim of refining docking calculations, we have subsequently performed a focused molecular docking of ADS-J1 onto the sole V3 loop of the three gp120 structures. The aim of these additional simulations was to identify the different interactions, if any, between ADS-J1 and gp120 before and after mutations. For the docking studies focused on the V3 loop, the following procedure was used. The grid box dimensions ($64 \times 126 \times 90$ Å with a grid spacing of 0.375 Å) were set in such a way to accommodate all amino acids of the V3 loop. A total of 100 runs were carried out for each simulation, using LGA with a population size of 200 and a maximum of 7.5×10^5 energy evaluations. A cluster analysis was carried out using 3 Å as the root-mean-square deviation tolerance. Finally, on the basis of the fact that Autodock does not perform any structural optimization and energy minimization of the complexes found, a molecular mechanics approach was applied to refine the Autodock output. The computational protocol applied consisted in the application of 10 000 steps of the steepest descent algorithm or lasted until the derivative convergence was 0.01 kcal/Å mol. AMBER* force fields with the continuum GB/SA solvation model (solvent water) as implemented in MacroModel were used during minimization. Moreover, because of the large number of atoms in the model, to correctly optimize the complexes obtained by the flexible docking, the following additional constraints had to be imposed: (*i*) A subset, comprising only the inhibitor and a shell of residues possessing at least one atom at a distance of 6 Å from any of the inhibitor atoms, was created and subjected to energy minimization. The inhibitor and all the amino acid side chains of the shell were unconstrained during energy minimization to allow for reorientation and proper hydrogen-bonding geometries and van der Waals contacts. (*ii*) All of the atoms not included in the above-defined subset were fixed, but their nonbond interactions with all of the relaxing atoms have been calculated. Further details on this computational protocol were reported elsewhere.[24]

The output structure of the minimization protocol were in turn rescored with Autodock to obtain the final values of their estimated free energy of binding.[23]

RESULTS AND DISCUSSION

Modeling the Interaction of ADS-J1 with gp120. The complete three-dimensional structure of gp120 is not available yet, from either experimental or theoretical sources. As a consequence, we have chosen to use the X-ray crystallographic structure of the monomeric core of gp120, complexed with the D1−D2 amino-terminal domains of CD4, as the input structure for computer simulations. This choice was guided by experimental data (time of drug addition) showing that ADS-J1 interfered with the gp120−coreceptor interactions, without interacting with the CXCR4 coreceptor,[8] thus suggesting that the molecular target of ADS-J1 was the gp120−CD4 complex.

However, it should be noted that the experimental sequence of gp120 presented two Gly−Ala−Gly tripeptide substitutions instead of both the V1/V2 loop residues 128−194 and the V3 loop residues 298−329. Moreover, residues constituting the V4 loop were all missed.

On the basis of these data, the first goal to be reached by a computational approach was the completion of the gp120 amino acid sequence and its structural optimization. For this purpose, V3 was computationally built starting from an experimental NMR structure, while the V4 loop was modeled by MD simulations starting from its primary sequence. Next, both the V3 and V4 loops were added to the core structure of gp120 and the resulting assembly was in turn optimized. On the other hand, both the V1 and V2 loops of gp120 were arbitrarily not modeled. This was due to the fact that experimental data on the inhibition properties of ADS-J1 clearly showed that the inhibitor preferentially induced mutations on the V3 and V4 loops, probably because of a direct interaction of ADS-J1 with these regions of gp120.[8] As a consequence, V1 and V2 loops were not expected to interact with the inhibitor and, thus, were not further considered in the calculations. Moreover, the literature reported that the binding of gp120 to CD4 prompts both V1 and V2 to "move out of the way" to expose shielded residues.[12] Considering that simulations of the gp120 assembly were performed taking into account the presence of a part of CD4, we assumed that V1 and V2 could be omitted from the calculations.

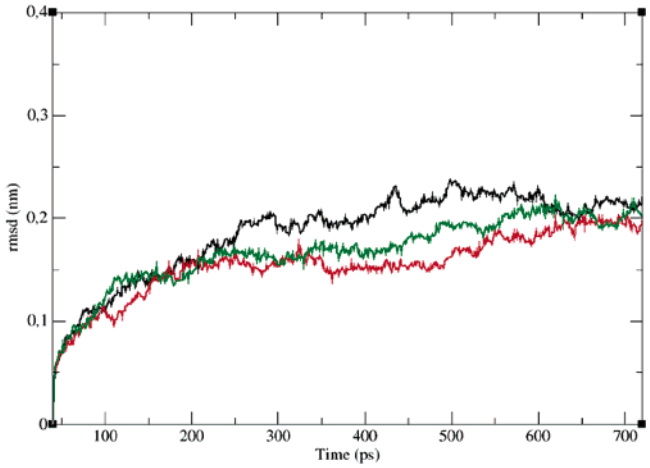

Figure 3. Graphical representation of the root-mean-square deviation (rmsd, expressed in nm and calculated on Cα atoms) versus simulation time for HIV-1 NL4-3wt (black line), NL4-3/AR177res (red line), and ARA49 (green line) gp120.

However, some differences were found by comparing the primary structure of the assembled gp120 with the sequence of NL4-3wt. As a consequence, we manually replaced the amino acids of the gp120 structure with the proper residues (namely, E269D, V275A, N340A, I423F, E429K, S461N, and E464G) to obtain the sequence corresponding to NL4-3wt. Analogously, the NL4-3/AR177res and ARA49 structures were obtained starting from NL4-3wt by replacement of the amino acids mutated in consequence of the treatment with AR177 and ADS-J1, respectively (see Figure 2 for details on mutations).

Finally, MD simulation protocols have been applied to the three sequences of gp120 (NL4-3wt, NL4-3/AR177res, and ARA49) to determine the optimal conformation of each structure.

Analysis of MD Simulations. MD simulations were performed on the complexes between CD4 and NL4-3wt and NL4-3/AR177res and ARA49, respectively. The results are graphically represented in Figure 3, showing the root-mean-square deviation (rmsd) calculated on the Cα atoms with respect to the starting coordinates. The rmsd of the protein

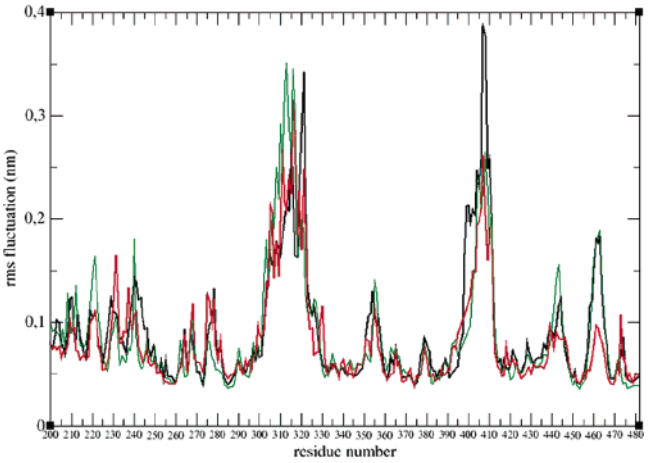

Figure 4. Graphical representation of the root-mean-square fluctuation (expressed in nm and calculated on Cα atoms) for residues 200−482 of HIV-1 NL4-3wt (black line), NL4-3/AR177res (red line), and ARA49 (green line) gp120.

Cα allows the checking of whether the protein reached the equilibration state during MD simulations. After the first 350 ps, the structure of NL4-3wt was fairly stable during the entire remaining time of MD simulation (Figure 3, black line), with a rmsd value of 0.21−0.23 nm calculated in comparison to the starting structure. A different profile was found for NL4-3/AR177res (Figure 3, red line). In fact, while the rmsd value increased to 0.18 nm during the first 550 ps, it stabilized until the end of the simulation. Similarly, while the rmsd of the ARA49 structure increased from 0.01 to 0.19 nm over the first 480 ps, after this time, the system stabilized around 0.19−0.21 nm (Figure 3, green line).

Although the representations reported in Figure 3 were useful in analyzing the dynamics of the whole protein structures, however, we were also interested in determining which parts of the protein were more flexible and how structural properties were influenced by the mutations. For this purpose, we also monitored the root-mean-square fluctuations of the Cα atoms (somewhat analogous to the crystallographic B factor) for each residue during MD simulations (Figure 4). Analysis of the plot generated for NL4-3wt (Figure 4, black line) showed that the larger fluctuations (rmsd > 0.2 nm) were mainly concentrated in the regions of the V3−V4 loops, corresponding to residues 312−316 and 319−322 (belonging to V3) and 399−411 (belonging to V4), with the highest fluctuation involving residue 321 (0.34 nm). Moreover, a mobility higher than 0.15 nm was observed for residues 460−463 belonging to the V5 loop. In principle, large fluctuations of the V3- and V4-loop residues during MD simulations were expected because their structures should be considered as computationally built theoretical models that were required to adapt their structure to the overall structure of gp120. However, when the equilibration phase was terminated, a significant flexibility of such regions remained, thus suggesting an intrinsic flexibility of these amino acid sequences in solution.

Moreover, similarly to that found for the NL4-3wt sequence, the plot for NL4-3/AR177res (Figure 4, red line) showed that residues affected by higher fluctuations were localized within both V3 and V4 loops. In fact, amino acids 305−306 and 310−322 (V3 loop) demonstrated high flexibility, with a maximum value of 0.32 nm corresponding to residue 316. In addition, regarding the V4−V5 loops, a flexibility lower than that of the wild type was observed. Several other differences can be evidenced within the V3 flexibility. As an example, residues 305 and 306, characterized by high flexibility on the NL4-3/AR177res protein, showed a reduced mobility on the wild-type structure.

An inspection of the residue mobility of ARA49 during MD simulations (Figure 4, green line) was worthy of further consideration, allowing us to highlight structural differences induced from amino acid mutations. In detail, mutated residues 320, 322, and 354 (all of them belonging to V3) showed reduced flexibility with respect to the corresponding amino acids of the wild type structure. Interestingly, the highly conserved GPGRAF motif of the V3 loop, corresponding to the 312−317 sequence, showed the highest flexibility of the entire loop, although it was not affected by any mutation. In fact, a rmsd of 0.35 nm was found for residues 313−316, while amino acid 312 showed a rmsd of 0.33 nm. Similarly to the NL4-3/AR177res protein, residues 399−411 of ARA49 (V4 loop) showed reduced flexibility with respect to NL43wt. Finally, fluctuations observed within the V5 loop were similar to that of NL43wt.

We are aware that the structures of NL4-3wt, NL4-3/AR177res, and ARA49 described here could be different from those involved in real biological processes. However, the application of reliable computational protocols gives assurance of obtaining plausible structures of NL4-3wt, NL4-3/AR177res, and ARA49 for subsequent calculations. In particular, upon building, MD simulations were performed with the aim of both optimizing the structures of the gp120 assemblies and (in particular) analyzing the conformational mobility of the most flexible regions such as the V3 and V4 loops.

Analysis of the Docked Complexes. On the basis of the fact that, in many case studies, Autodock 3.0 was demonstrated to be able to find the correct protein/ligand complex without any prior knowledge of the binding site,[25] we have chosen to use such software as the molecular docking tool to explore the binding mode of the inhibitor and to evaluate its binding conformations within the NL4-3/AR177res gp120 structure, corresponding to the strain used to evaluate the anti-HIV-1 resistance to ADS-J1. In particular, two different docking protocols and an energy minimization step were applied in sequence. First, a blind docking procedure was set up with the aim of finding the preferred binding site(s) of ADS-J1 onto the assembled gp120 structure. The blind docking on the whole surface of NL4-3/AR177res was performed keeping the best 150 conformations, as ranked by the docking software. As a result of the blind docking, the conformers with the lower energy of binding were found to bind gp120 at the level of the V3 loop (Figure 5A). These findings were in good agreement with experimental data showing the V3 loop as the preferential binding site for ADS-J1. Next, on the basis of the fact that the V3 loop was suggested by both experimental results and blind docking simulations as the preferred binding site for ADS-J1, a focused docking protocol was applied with the purpose of obtaining more refined complexes. Finally, considering that docking simulations were performed with the protein as a rigid body and any structural optimization and energy minimization of the complexes were done by Autodock, a molecular mechanics approach was applied to refine and

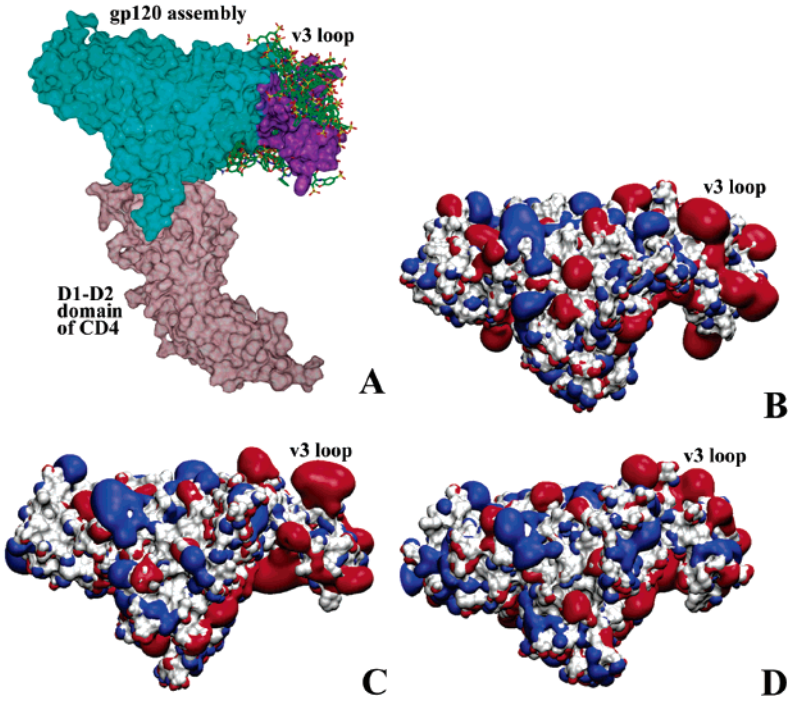

Figure 5. (A) Graphical representation of results from blind docking simulations of ADS-J1 (displayed following the atom-type color code) onto the HIV-1 NL4-3/AR177res gp120 model (cyan). Conformers with the lowest energy of binding were found to bind the V3 loop of the assembled gp120 structure. D1−D2 domains of CD4 were also represented (pink). (B−D). Electrostatic potential maps generated by means of Autogrid software for the HIV-1 NL4-3wt (B), NL4-3/AR177res (C), and ARA49 (D) gp120 models. Positive potentials (red) were mapped at +0.5 kcal/mol; negative potentials (blue) were mapped at −0.5 kcal/mol. It is important to note that extended regions of positive potentials were found in correspondence to the V3 loop of both NL4-3wt (B) and NL4-3/AR177res (C). Differently, maps for the ARA49 sequence (D) showed either the reduction of positive potential regions or the appearance of significantly large negative potential volumes.

optimize the conformations chosen among the docked structures.

Binding Mode of ADS-J1 onto NL4-3wt and NL4-3/AR177res. On the basis of the fact that computational simulations suggested the V3 loop as the preferential binding site for ADS-J1 onto NL4-3/AR177res, focused molecular docking calculations were performed onto the sole V3 loop of gp120. Such calculations were set to check if differences existed in the binding mode of ADS-J1 before and after mutations. An analysis of the results derived by docking ADS-J1 onto V3 of NL4-3wt showed several clusters constituted by a comparable number of conformations. As a consequence, the minimum energy conformer (with an estimated free energy of binding of −21.0 kcal/mol) has been chosen as the best conformation docked to the wild type sequence. Within the structure of this complex (Figure 6A), very good interactions between the ligand and the macromolecule, were found. Particularly, Lys305, Arg304, Asn325, Thr297, Val318, and Gly314 established hydrogen-bond contacts with the ligand. Moreover, the complex was highly stabilized by electrostatic interactions between the sulfonate groups of the inhibitor and several charged residues (namely, Lys305, Arg304, and Arg327) of the protein. Finally, Ile323 and the aliphatic portion of the Lys305 side chain interacted with the ligand through positive van der Waals contacts.

In a similar way, the complex between the minimum energy conformer of ADS-J1 (with an estimated free energy of binding of −20.0 kcal/mol) and NL43/AR177res was stabilized by a network of hydrogen bonds between the ligand and Lys305, Gln442, Thr303, Asn325, Ser306, and Gln322 (Figure 6B). Electrostatic interactions involving the sulfonate groups and positively charged amino acids, such as Lys305, contributed significantly to the stabilization of the complex. Moreover, hydrophobic contacts between the aromatic side chain of Tyr300 and both the anilino moiety and the triazine ring of the ligand were found. Finally, Ile309 and the polymethylene chain of Lys305 interacted with the ligand through positive van der Waals contacts.

A comparison of the complexes between ADS-J1 and NL4-3wt and NL4-3/AR177res showed a series of common interactions between the ligand and each of the macromolecules. This finding suggested that ADS-J1 was characterized by stereoelectronic properties allowing the ligand to interact in a similar way (i.e., with a comparable affinity) with both the protein structures. In fact, profitable contacts between the ligand and residues such as Lys305 and Asn325 were found in both the complexes, suggesting that the above amino acids could play a crucial role in defining the interaction pathway between ADS-J1 and gp120.

To summarize the docking results, ADS-J1 was able to preferably and profitably bind the V3 loop of gp120, in good agreement with experimental data.

Binding Mode of ADS-J1 onto ARA49. The most important consequence of mutations on gp120 was the reduction of the positive charge on the V3 loop, leading to a deep change of the electrostatic potential on the protein surface. By means of the Autogrid software, electrostatic potentials were calculated for the protein surface and the corresponding maps were visualized to graphically appreciate regions of positive and negative potential. Figure 5 clearly showed that the V3 loop of gp120 is rich in positively charged amino acids. However, the above-described muta-

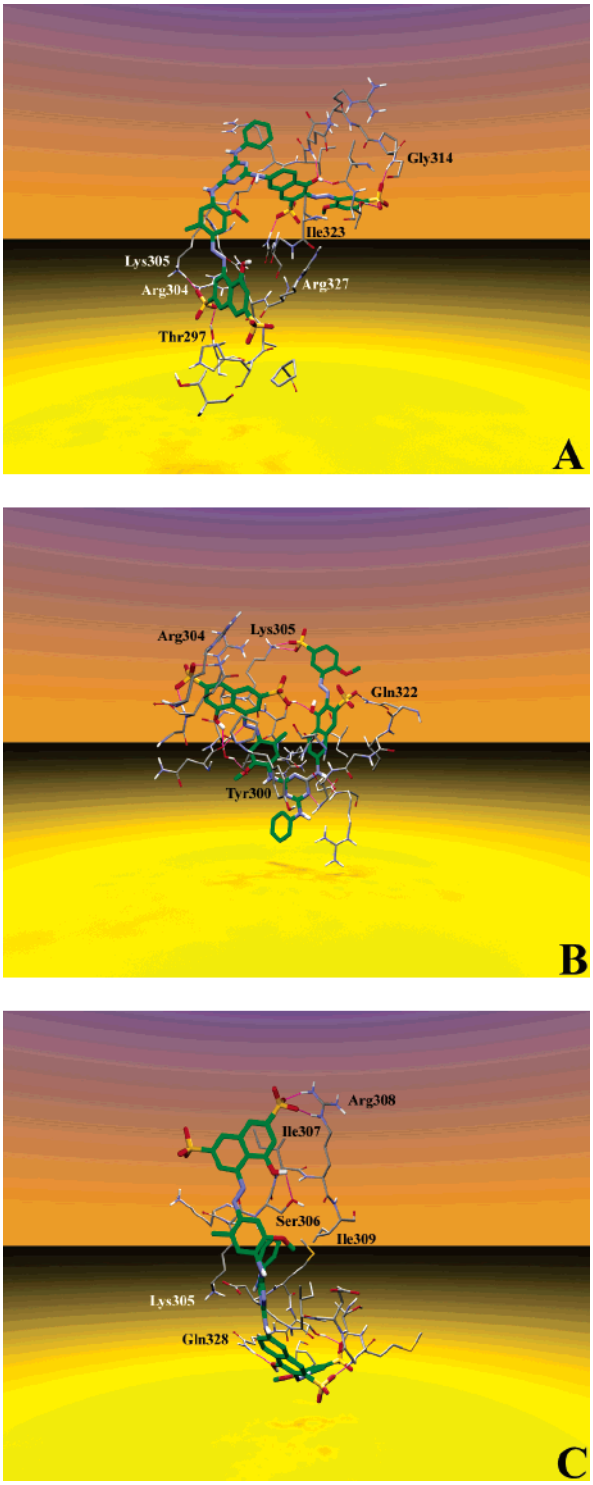

Figure 6. ADS-J1 (green) in complex with the V3 loop of HIV-1 NL4-3wt (A), NL4-3/AR177res (B), and ARA49 (C). For the sake of clarity, nonpolar hydrogens were omitted, hydrogen-bond interactions are represented by pink lines, and only a portion of the V3 loop is displayed.

tions led to a marked decrease of the positive charge of the protein surface, causing a decreased affinity of the ligand for the protein. Moreover, it is also important to note that, within the entire gp120, the V3 loop remained the region with the highest positive charge, also upon mutations.

Docking simulations of ADS-J1 onto ARA49 led to the identification of the most populated cluster as constituted by six conformers. Among them, the first ranked conformation showed an estimated free energy of binding of −14 kcal/mol and interacted with the protein as summarized in Figure 6C. Hydrogen bonds were found between ADS-J1 and Arg308, Ser306, Thr327, and Gln328. Moreover, Ile307, Ile309, Ile323, Met326, and the aliphatic portion of Lys305 interacted with the ligand through positive van der Waals contacts. Such interactions appeared to contribute to the complex stabilization less than those found for complexes with NL4-3wt and NL4-3/AR177res. Interestingly, Lys305, involved in a hydrogen bond contributing to the stabilization of the other complexes, interacted with the mutated Asp325 of ARA49.

A comparison of the complex ADS-J1/ARA49 and the structures of both ADS-J1/NL4-3wt and ADS-J1/NL4-3/AR177res allowed justification of the lower affinity of ADS-J1 toward ARA49 (with respect to the other two proteins) on the basis of a reduced network of hydrogen bonds and a decrease in electrostatic profitable contacts. Such an evaluation can be performed by decomposing the binding free energy of the inhibitor as electrostatic and nonelectrostatic parts. In fact, from the analysis of the AutoDock scoring function terms (van der Waals, electrostatic, hydrogen bond, loss of entropic term—i.e., torsional freedom—, and desolvation contributions), it can be estimated that, while electrostatic interactions contributed about 5.3 and 4.3 kcal/mol in the complexes ADS-J1/NL4-3wt and ADS-J1/NL4-3/AR177res, respectively, the average electrostatic contribution to the ADS-J1/ARA49 binding was reduced to 2.9 kcal/mol. This finding suggested that the reduced affinity of ADS-J1 toward ARA49 was mainly due to a marked reduction of electrostatic contacts and hydrogen bonding (while van der Waals contributions were comparable for all three complexes), which in turn decreased when mutations occurred. This is in agreement with the structural properties of the V3 binding pocket, whose positive charge was reduced from 9 to 5 upon mutations.

However, the binding mode of the ligand with ARA49 showed several interactions also found in the other complexes, such as the van der Waals contacts with Lys305, Ile309, and Ile323 and a hydrogen-bond interaction with Ser306. On the contrary, the interactions with Lys305, Asn325, Arg304, and Gln322, found to be crucial for the stabilization of the other complexes, were lost, as a result of the mutations that occurred, with a consequent lack of complex stability and lower affinity.

CONCLUSIONS

Experimental data together with results from MD and molecular docking simulations allowed understanding of the mechanism by which ADS-J1 inhibited HIV-1 viruses. The development of resistance through serial cultures of NL4-3/AR177-resistant HIV-1 in the presence of ADS-J1 rendered a virus containing a putative site of mutated residues preferentially located in the V3 loop of gp120, indicating it as the target for this inhibitor. In agreement with experimental data, the results of blind docking on the whole surface of gp120 suggested that the V3 loop was the preferential binding site for ADS-J1 onto NL4-3/AR177res. The virus would overcome the inhibitory activity by modifying the electrostatic potential of the basic face of gp120. Selection of the ADS-J1-resistant virus induced a reduction of the net charge

from +9 to +5 in the V3 loop amino acid sequence and a subsequent alteration of the stereoelectronic properties of the gp120 surface. As a consequence, a marked decrease in the electrostatic component of the binding energy of the inhibitor was also calculated, leading to a ADS-J1/ARA49 complex less stabilized with respect to the complexes between the same inhibitor and NL4-3wt and NL4-3/AR177res. Moreover, the dynamics of NL43wt, as well as those of its mutants NL43/AR177res and ARA49, all in complex with CD4, were also analyzed. As expected, the V3 loop was found to be characterized by a very high flexibility, known to play an important role for the activity of gp120.

ACKNOWLEDGMENT

This study was partially supported by grants from the European TRIoH Consortium (LSHB-2003-503480), the Spanish Ministerio de Ciencia y Tecnología Project BFI-2003-00405, and the Catalan Fundació La Marató de TV3 project 020930. M.B. thanks the Merk Research Laboratories (2004 Academic Development Program Chemistry Award). F.M. thanks the Divisione di Chimica Farmaceutica della Società Chimica Italiana and Farmindustria for the ''Premio Farmindustria 2004" award.

REFERENCES AND NOTES

(1) Blair, W. S.; Lin, P.-F.; Meanwell, N. A.; Wallace, O. B. HIV-1 entry − an expanding portal for drug discovery. *Drug Discovery Today* **2000**, *5*, 183−194.

(2) Kowalski, M.; Potz, J.; Basiripour, L.; Dorfman, T.; Goh, W. C.; Terwilliger, E.; Dayton, A.; Rosen, C.; Haseltine, W.; Sodroski, J. Functional regions of the envelope glycoprotein of human immunodeficiency virus type 1. *Science* **1987**, *237*, 1351−1355.

(3) Wyatt, R.; Sodroski, J. The HIV-1 envelope glycoproteins: fusogens, antigens, and immunogens. *Science* **1998**, *280*, 1884−1888.

(4) Este, J. A. Virus Entry as a Target for Anti-HIV Intervention. *Curr. Med. Chem.* **2003**, *10*, 1617−1632.

(5) Manetti, F.; Corelli, F.; Mongelli, N.; Lombardi Borgia, A.; Botta, M. Research on anti-HIV-1 agents. Investigation on the CD4-Suradista binding mode through docking experiments. *J. Comput.-Aided Mol. Des.* **2000**, *14*, 355−368.

(6) Vives, R. R.; Imberty, A.; Sattentau, Q. J.; Lortat-Jacob, H. Heparan sulfate targets the HIV-1 envelope glycoprotein gp120 coreceptor binding site. *J. Biol. Chem.* **2005**, *22*, 21353−21357.

(7) Moulard, M.; Lortat-Jacob, H.; Mondor, I.; Roca, G.; Wyatt, R.; Sodroski, J.; Zhao, L.; Olson, W.; Kwong, P. D.; Sattentau, Q. J. Selective Interactions of Polyanions with Basic Surfaces on Human Immunodeficiency Virus Type 1 gp120. *J. Virol.* **2000**, *74*, 1948−1960.

(8) Armand-Ugón, M.; Clotet-Codina, I.; Tintori, C.; Manetti, F.; Clotet, B.; Botta, M.; Esté, J. A. The anti-HIV activity of ADS-J1 targets the HIV-1 gp120. *Virology* **2005**, *343*, 141−149.

(9) Debnath, A. K.; Radigan, L.; Jiang, S. Structure-based identification of small molecule antiviral compounds targeted to the gp41 core structure of the human immunodeficiency virus type 1. *J. Med. Chem.* **1999**, *42*, 3203−3209.

(10) Armand-Ugon, M.; Gutierrez, A.; Clotet, B.; Este, J. A. HIV-1 resistance to the gp41-dependent fusion inhibitor C-34. *Antiviral Res.* **2003**, *59*, 137−142.

(11) Kwong, P. D.; Wyatt, R.; Majeed, S.; Robinson, J.; Sweet, R. W.; Sodroski, J.; Hendrickson, W. A. Structures of HIV-1 gp120 Envelope Glycoproteins from Laboratory-Adapted and Primary Isolates. *Structure* **2000**, *8*, 1329−39.

(12) Pan, Y.; Ma, B.; Keskin, O.; Nussinov, R. Characterization of the conformational state and flexibility of HIV-1 glycoprotein gp120 core domain. *J. Biol. Chem.* **2004**, *279*, 30523−30530.

(13) *MacroModel*, version 8.5.; Schrodinger, LLC: Portland, OR, 2003.

(14) Vranken, W. F.; Budesinsky, M.; Fant, F.; Boulez, K.; Borremans, F. A. M. The complete Consensus V3 loop peptide of the envelope protein gp120 of HIV-1 shows pronounced helical character in solution. *FEBS Lett.* **1995**, *374*, 117−121.

(15) Notredame, C.; Higgins, D.; Heringa, J. T-Coffee: A novel method for multiple sequence alignments. *J. Mol. Biol.* **2000**, *302*, 205−217.

(16) Schwede, T.; Kopp, J.; Guexand, N.; Peitsch, M. C. SWISS-MODEL: an automated protein homology-modeling server. *Nucleic Acids Res.* **2003**, *13*, 3381−5. Further details can be found on the web page http://swissmodel.expasy.org.

(17) Menendez-Arias, L.; Este, J. A. HIV-resistance to viral entry inhibitors. *Curr. Pharm. Des.* **2004**, *10*, 1845−60

(18) Kalé, L.; Skeel, R.; Bhandarkar, M.; Brunner, R.; Gursoy, A.; Krawetz, N.; Phillips, J.; Shinozaki, A.; Varadarajan, K.; Schulten. K. NAMD2: Greater scalability for parallel molecular dynamics. *J. Comput. Phys.* **1999**, *151*, 283−312.

(19) MacKerell, A. D., Jr.; Bashford, D.; Bellott, R. L.; Dunbrack, R. L., Jr.; Evanseck, J. D.; Field, M. J.; Fischer, S.; Gao, J.; Guo, H.; Ha, S.; Joseph-McCarthy, D.; Kuchnir, L.; Kuczera, K.; Lau, F. T. K.; Mattos, C.; Michnick, S.; Ngo, T.; Nguyen, D. T.; Prodhom, B.; Reiher, W. E., III; Roux, B.; Schlenkrich, M.; Smith, J. C.; Stote, R.; Straub, J.; Watanabe, M.; Wiorkiewicz-Kuczera, J.; Yin, D.; Karplus, M. All-Atom Empirical Potential for Molecular Modeling and Dynamics Studies of Proteins *J. Phys. Chem. B* **1998**, *102*, 3586−3616.

(20) van der Spoel, D.; van Drunen, R.; Berendsen, H. J. C. Groningen machine for chemical simulations. Groningen: Department of Biophysical Chemistry, BIOSON Research Institute Nijenborgh 4 NL-9717 AG, 1994.

(21) Morris, G. M.; Goodsell, D. S.; Halliday, R. S.; Huey, R.; Hart, W. E.; Belew, R. K.; Olson, A. J. Automated Docking Using a Lamarckian Genetic Algorithm and Empirical Binding Free Energy Function. *J. Comput. Chem.* **1998**, *19*, 1639−1662.

(22) Ren, J.; Esnouf, R.; Garman, E.; Somers, D.; Ross, C.; Kirby, I.; Keeling, J.; Darby, G.; Jones, Y.; Stuart, D. High-resolution structures of HIV-1 RT from four RT-inhibitor complexes. *Nat. Struct. Biol.* **1995**, *2*, 293−302.

(23) Ragno, R.; Mai, A.; Massa, S.; Cerbara, I.; Valente, S.; Bottoni, P.; Scatena, R.; Jesacher, F.; Loidl, P.; Brosch, G. 3-(4-Aroyl-1-methyl-1*H*-pyrrol-2-yl)-N-hydroxy-2-propenamides as a New Class of Synthetic Histone Deacetylase Inhibitors. 3. Discovery of Novel Lead Compounds through Structure-Based Drug Design and Docking Studies. *J. Med. Chem.* **2004**, *47*, 1351−1359.

(24) Cona, A.; Manetti, F.; Leone, R.; Corelli, F.; Tavladoraki, P.; Polticelli, F.; Botta, M. Molecular Basis for the Binding of Competitive Inhibitors of Maize Polyamine Oxidase. *Biochemistry* **2004**, *43*, 3426−3435.

(25) Hetenyl, C.; Van Der Spoel, D. Efficient docking of peptides to proteins without prior knowledge of the binding site. *Protein Sci.* **2002**, *11*, 1729−1737.

CI050414H